



# A pH-Neutral, Metal-Free Aqueous Organic Redox Flow Battery Employing an Ammonium Anthraquinone Anolyte

Bo Hu<sup>+</sup>, Jian Luo<sup>+</sup>, Maowei Hu, Bing Yuan und T. Leo Liu\*

Dedicated to Dr. Daniel L. DuBois and Prof. Mary Rakowski DuBois on the occasion of their 70<sup>th</sup> birthday

**Abstract:** Redox-active anthraquinone molecules represent promising anolyte materials in aqueous organic redox flow batteries (AORFBs). However, the chemical stability issue and corrosion nature of anthraquinone-based anolytes in reported acidic and alkaline AORFBs constitute a roadblock for their practical applications in energy storage. A feasible strategy to overcome these issues is migrating to pH-neutral conditions and employing soluble AQDS salts. Herein, we report the 9,10-anthraquinone-2,7-disulfonic diammonium salt AQDS-(NH<sub>4</sub>)<sub>2</sub> as an anolyte material for pH-neutral AORFBs with solubility of 1.9 M in water, which is more than 3 times that of the corresponding sodium salt. Paired with an NH<sub>4</sub>I catholyte, the resulting pH-neutral AORFB with an energy density of 12.5 Wh L<sup>-1</sup> displayed outstanding cycling stability over 300 cycles. Even at the pH-neutral condition, the AQDS(NH<sub>4</sub>)<sub>2</sub>/NH<sub>4</sub>I AORFB delivered an impressive energy efficiency of 70.6 % at 60 mA cm<sup>-2</sup> and a high power density of 91.5 mW cm<sup>-2</sup> at 100 % SOC. The present AQDS(NH<sub>4</sub>)<sub>2</sub> flow battery chemistry opens a new avenue to apply anthraquinone molecules in developing low-cost and benign pH-neutral flow batteries for scalable energy storage.

## Introduction

Extensive consumption of fossil fuels within last two hundred years has resulted in the dramatic increase of the concentration of CO<sub>2</sub> in the atmosphere from 280 ppm at the beginning of the industrial revolution in the 19<sup>th</sup> century to about 408 ppm in 2018.<sup>[1]</sup> Nowadays, utilization of renewable energy resources such as solar and wind energy has been recognized to be a sustainable and environmentally benign strategy to alleviate the world's severe dependency on traditional fossil fuels, and thus enables environmental recovery and sustainable economic development of our society.<sup>[2]</sup> In order to manage the intermittent and fluctuating nature of solar and wind energy, cost-effective technologies for energy

conversion and storage are in urgent need.<sup>[3]</sup> Among the numerous energy storage technologies, redox flow batteries (RFBs) have been recognized as a promising technology to overcome the intermittency of renewable energy and supply reliable electricity to electricity grids with a scale up to MW/MWh.<sup>[3]</sup>

The unique cell design of RFBs empowers a number of attractive technical merits for large-scale energy storage in comparison to traditional static rechargeable batteries, such as safe operation, excellent scalability, unique decoupled energy/power capability, high current operation, and high power output.<sup>[3a,b]</sup> As one of the most advanced RFB technologies, vanadium redox flow battery (VRFB) has received the most commercializing attempts.<sup>[3a]</sup> Nevertheless, its wide adoption is still limited by the high active material cost, low earth abundance for vanadium, and strong acid based hazardous electrolyte.<sup>[3b,c]</sup> To overcome these technical challenges, we and other groups have developed aqueous organic RFBs (AORFBs) and nonaqueous organic RFBs (NAORFBs)<sup>[4]</sup> employing more sustainable and abundant redox active organic molecules, such as viologen,<sup>[5]</sup> metallocene,<sup>[5d,6]</sup> pyridinium,<sup>[7]</sup> quinone,<sup>[8]</sup> (2,2,6,6-tetramethylpiperidin-1-yl)oxyl (TEMPO),<sup>[5a,c,f,9]</sup> phenazine derivatives,<sup>[10]</sup> and other molecular designs.<sup>[11]</sup> Among the various redox active molecules, viologen<sup>[5]</sup> and anthraquinone (AQ)<sup>[8a-c]</sup> have been extensively studied as anolytes in AORFBs. So far viologen based pH neutral AORFBs have demonstrated most stable cycling performance as the pH neutral condition suppresses side reactions for active species caused by protons and hydroxides at acidic and alkaline conditions.<sup>[5]</sup> However, AQ molecules have been primarily studied in acidic or alkaline AORFBs<sup>[8a-c]</sup> and subject to chemical degradation at either acidic or alkaline conditions.<sup>[12]</sup> First, side reactions under acidic conditions (such as bromination and acid catalyzed reactions) lead to capacity decay.<sup>[12a,b]</sup> Second, the redox potential of AQ molecules such as AQDSH<sub>2</sub> positively shifts to +0.21 V vs. SHE in acidic electrolytes, dramatically limiting the open circuit voltage for the whole battery. Third but not the last, acidic supporting electrolytes and bromine based catholyte are highly corrosive and hazardous. Other anthraquinone derivatives have also been studied in alkaline AORFBs but still suffer chemical degradation,<sup>[12c]</sup> a major cause for capacity decay, low solubility and high cost.<sup>[8b,d]</sup> Deteriorative impacts of acidic or alkaline conditions are also applied to catholyte molecules.<sup>[8f,13]</sup> For example, K<sub>4</sub>Fe(CN)<sub>6</sub> as the most common cathode material in alkaline AORFBs is not chemically stable at alkaline conditions as recently examined in a half-cell flow battery study.<sup>[13]</sup>

[\*] B. Hu,<sup>[†]</sup> J. Luo,<sup>[†]</sup> M. Hu, T. L. Liu  
Department of Chemistry and Biochemistry, Utah State University  
0300 Old Main Hill, Logan, UT 84322 (USA)  
E-Mail: leo.liu@usu.edu

B. Yuan  
State Key Laboratory Base of Eco-chemical Engineering, College of  
Chemistry and Molecular Engineering, Qingdao University of Science  
and Technology  
Qingdao 266042 (China)

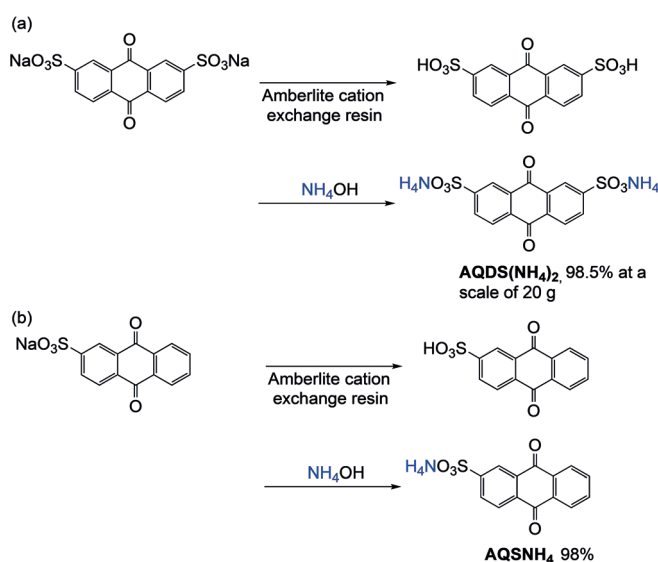
[†] These authors contributed equally to this work.

Supporting information and the ORCID identification number(s) for the author(s) of this article can be found under <https://doi.org/10.1002/anie.201907934>.

Thus, we have become promoted to investigate AQ molecules at pH neutral conditions to address these technical issues observed in AQ based acidic and alkaline AORFBs and achieve improved cycling performance. 9,10-anthraquinone-2,7-disulfonic acid (AQDSH<sub>2</sub>) represents one of the most inexpensive AQ anolyte candidates and was first applied in strongly acidic AORFBs.<sup>[8a,e]</sup> Intuitively, the sodium salt of sulfonated anthraquinone derivatives is the first class of candidates to be investigated. 9,10-anthraquinone-2-sulfonic acid sodium salt (AQSNa) and 9,10-anthraquinone-2,7-disulfonic acid disodium salt (AQDSNa<sub>2</sub>) maintain many merits of the acid compound (e.g. extraordinary stability, fast redox kinetics, and widespread commercial availability). However, we found both AQSNa and AQDSNa<sub>2</sub> have much lower solubility in water at pH 7 (less than 30 mM for AQDSNa and 0.58 M for AQDSNa<sub>2</sub> in water) which limits the capacity and energy density of these AQ molecule based pH neutral AORFBs. Only a very few studies have been reported in improving their solubility for neutral AORFB applications. One example is employing ethylene glycol as additives to increase the solubility of AQDSNa<sub>2</sub>.<sup>[14]</sup> Recently, an ethylene oxide functionalized AQ demonstrated high solubility at pH neutral conditions but is not chemically stable.<sup>[15]</sup> A previous study also showed hydrophilic tetrakis-(hydroxymethyl)-phosphonium cations (TKMP) can largely increase the solubility of 1,2-dihydroxy-9,10-anthraquinone-3-sulfonate (Alizarin) at pH neutral conditions.<sup>[16]</sup> However, Alizarin-TKMP showed poor electrochemical behaviors and has not been demonstrated in flow battery studies. Herein, we report the synthesis, spectroscopic, and electrochemical studies of a highly soluble ammonium cation functionalized AQ molecule, **AQDS(NH<sub>4</sub>)<sub>2</sub>** (1.9 M in H<sub>2</sub>O, and 1.3 M in 1.0 M NH<sub>4</sub>I). An **AQDS(NH<sub>4</sub>)<sub>2</sub>/NH<sub>4</sub>I** pH neutral AORFB with an energy density of 12.5 WhL<sup>-1</sup> delivered very stable cycling performance in a pH neutral AORFB for 300 cycle and an outstanding energy efficiency of 70.6% at 60 mA cm<sup>-2</sup>.

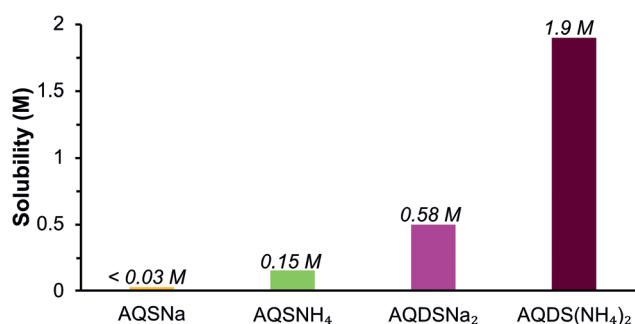
## Results and Discussion

Our group reported a molecular engineering study of ferricyanide and ferrocyanide catholytes for pH neutral AORFB applications using a straightforward strategy of cation modulation.<sup>[5h]</sup> The newly designed neutral (NH<sub>4</sub>)<sub>3</sub>Fe(CN)<sub>6</sub> and (NH<sub>4</sub>)<sub>4</sub>Fe(CN)<sub>6</sub> catholytes manifest much higher solubility than their sodium and potassium salts and retain comparable chemical stability. Inspired by the ammonium cation effect to improve the solubility of ferricyanide and ferrocyanide compounds, we adopted the same strategy to AQSNa and AQDSNa<sub>2</sub> salts. By replacing the counter cation Na<sup>+</sup> with NH<sub>4</sub><sup>+</sup>, a solubility increase and chemical stability maintainability were anticipated. The desired anthraquinone sulfonic acid ammonium salts, **AQSNH<sub>4</sub>** and **AQDS(NH<sub>4</sub>)<sub>2</sub>**, were synthesized by a straightforward two-step route with high yields (Scheme 1). The first reaction is the ion exchange reaction using Amberlite cation exchange resin to convert the sodium salts to AQSH and AQDSH<sub>2</sub>. Then the second step is an acid/base reaction of AQDSH<sub>2</sub> (or AQSH) with NH<sub>4</sub>OH to produce the target ammonium salts. The synthesis of



**Scheme 1.** Synthesis of (a) **AQDSNH<sub>4</sub>** and (b) **AQS(NH<sub>4</sub>)<sub>2</sub>**.

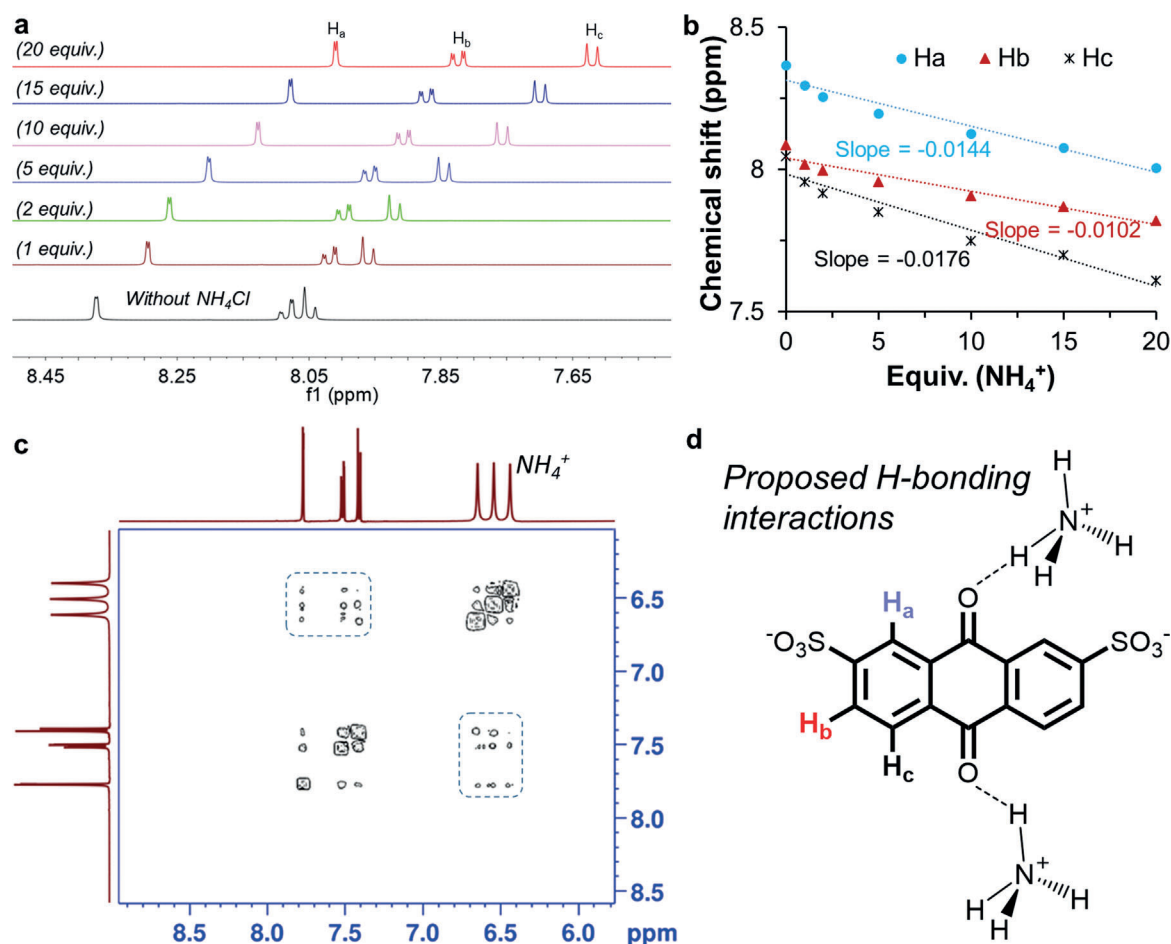
**AQDS(NH<sub>4</sub>)<sub>2</sub>** was demonstrated at a scale of 20 g with an excellent yield of 98.5% (Scheme 1). UV/Vis measurements were conducted to determine the solubility of **AQSNH<sub>4</sub>** and **AQDS(NH<sub>4</sub>)<sub>2</sub>**. In agreement with our expectation, both ammonia salts showed much higher solubility compared to their sodium forms (Figure 1). **AQSNH<sub>4</sub>** can be dissolved in water



**Figure 1.** A comparison of the solubility of AQSNa (yellow), **AQSNH<sub>4</sub>** (green), and AQDSNa<sub>2</sub> (purple), and **AQDS(NH<sub>4</sub>)<sub>2</sub>** (brown).

up to 0.15 M while the AQSNa is barely soluble (less than 30 mM). Surprisingly, **AQDS(NH<sub>4</sub>)<sub>2</sub>** displayed a remarkable solubility of 1.9 M in water which is nearly 4 times of that of **AQDSNa<sub>2</sub>** (0.58 M in water). Even in 1.0 M NH<sub>4</sub>I supporting electrolyte, the solubility still can reach 1.3 M. To the best of our knowledge, this is one of the most water-soluble anthraquinone derivatives at the pH neutral condition.

We hypothesized that the boosted solubility was attributed to two reasons. On the one hand, the hydrophilic property of ammonium cation facilitates the dissolving of the salt in water as reported in our previous work.<sup>[5h]</sup> On the other hand, hydrogen bonds formed among NH<sub>4</sub><sup>+</sup> cation and AQDS anion, is believed to enhance the solvation of AQDS anions in water, thus improving its solubility. In order to obtain evidences for these hydrogen-bonding interactions, Nuclear magnetic resonance (NMR) titration studies of AQDSNa<sub>2</sub>



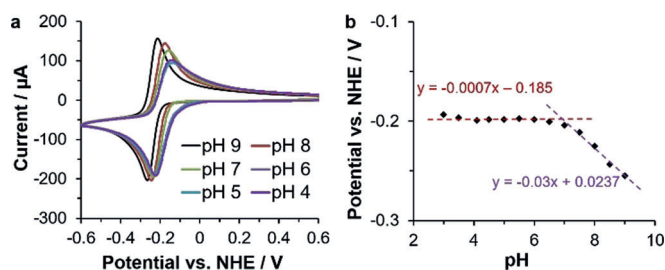
**Figure 2.** (a)  $^1\text{H}$  NMR titration of 50 mM  $\text{AQDSNa}_2$  in  $\text{D}_2\text{O}$  with various equivalents of  $\text{NH}_4\text{Cl}$  from 1 to 20. Ammonium hydroxide solution was used to adjust the pH value to 7.0. (b) Relationship between  $^1\text{H}$ -NMR chemical shift and the equivalent of ammonium. (c) 2D NMR (COSY) spectrum of 0.1 M  $\text{AQDS}(\text{NH}_4)_2$  in  $\text{D}_2\text{O}$ , pH was adjusted to 3 to guarantee the observation of ammonium cation in the spectrum. (d) Schematic hydrogen bonding interactions proposed for  $\text{AQDS}(\text{NH}_4)_2$ .

were performed with the addition of  $\text{NH}_4\text{Cl}$  as the ammonium source (Figure 2a). The pH value of each NMR sample was adjusted to 7.0 to avoid the possible chemical shift drift due to the change of pH values. As a result of the  $\text{NH}_4\text{Cl}$  titration, a noticeable upfield shift of the  $^1\text{H}$ -NMR signals of  $\text{AQDS}^{2-}$  moiety was observed as shown in Figure 2a. Protons,  $\text{H}_a$  and  $\text{H}_c$ , experienced relative large chemical shift while the proton  $\text{H}_b$ , far from the carbonyl oxygen atoms, displayed the smallest signal shift ( $-0.0102$  ppm/equiv  $\text{NH}_4\text{Cl}$ ). The observed upfield shift is interpreted as that the hydrogen bonding of the  $\text{NH}_4^+$  cations with the carbonyl oxygen can disrupt the pi-electron delocalization of the center ring with two outside rings and thus reduce the electron-withdrawing effect of the pi-electrons of the carbonyl groups.<sup>[17]</sup> The observations indicate the hydrogen bonding interactions between the carbonyl oxygen atom and  $\text{NH}_4^+$  cations (Figure 2d). This is in line with the  $^{13}\text{C}$  NMR signal upfield shift of  $\text{AQDS}(\text{NH}_4)_2$  compared to  $\text{AQDSNa}_2$  (see Figure S2). Specifically, the  $^{13}\text{C}$  resonances of carbon atoms at position 9 and 10 showed upfield shift while other carbons barely had any changes. In the 2D NMR (COSY) spectrum (Figure 2c), the strong interaction between the proton of ammonium and the protons of

$\text{AQDS}$  was also observed and highlighted by the blue dash rectangles in Figure 2C, providing another strong evidence for the formation of hydrogen-bonds. In addition, a control experiment was conducted by titrating sodium 2,4-dimethylbenzenesulfonate with  $\text{NH}_4\text{Cl}$  (Figure S4). In this case, no chemical shift was observed with the  $\text{NH}_4^+$  concentration increase, further proving that the hydrogen bonds form on the carbonyl oxygen atoms other than sulfonate oxygen atoms. The similar trend was also observed for  $\text{AQSSNa}$  by the same  $\text{NH}_4\text{Cl}$  titration (Figure S3).

The synthesized  $\text{AQDS}(\text{NH}_4)_2$  was proved to be not only highly soluble in water but also chemically stable even at an elevated temperature and pH neutral conditions. After the treatment of an NMR sample of  $\text{AQDS}(\text{NH}_4)_2$  in  $\text{D}_2\text{O}$  at  $80^\circ\text{C}$  for 2 weeks,  $^1\text{H}$  NMR studies indicated no chemical decomposition (Figure S5), representing a desired chemical characteristic for flow battery applications.

The ensuing studies were directed on the electrochemical behaviors of  $\text{AQDS}(\text{NH}_4)_2$ . Cyclic voltammetry studies revealed a pair of reversible redox peaks at  $-0.20$  V vs. NHE in 0.5 M  $\text{NH}_4\text{I}$  electrolyte at pH 7 (Figure 3a), which is ca. 410 mV more negative than that of  $\text{AQDSH}_2$  at acidic con-



**Figure 3.** (a) Cyclic voltammograms of  $\text{AQDS}(\text{NH}_4)_2$  at various pH conditions. (b) Pourbaix diagram of  $\text{AQDS}(\text{NH}_4)_2$  in 0.5 M  $\text{NH}_4\text{l}$  solution. Conditions: 4.0 mM analyte in 0.5 M  $\text{NH}_4\text{l}$  electrolyte; scan rate:  $100 \text{ mVs}^{-1}$ ; working electrode, glassy carbon electrode; counter electrode, glassy carbon; reference electrode, Ag/AgCl. The pH value was adjusted using ammonium hydroxide solution. FcNCl (0.60 V vs. NHE at pH 7)<sup>[5d]</sup> was used to calibrate the redox potential.

ditions. In addition, compared to AQ molecules ( $< -0.45 \text{ V}$  vs. NHE) used in alkaline AORFBs,<sup>[8b-d]</sup> the redox potential of  $\text{AQDS}(\text{NH}_4)_2$  ( $-0.2 \text{ V}$  vs. NHE) is much less negative and thus its reduced state is more oxygen tolerant. The thermodynamic potentials of proton-coupled electron transfer (PCET) redox reactions of anthraquinone molecules are well known to be pH dependent, especially in the near neutral region (pH 3–9).<sup>[8a]</sup> The general electrochemical reaction of  $\text{AQDS}^{2-}$  is shown in Equation (1), where two electrons were transferred while various number ( $0 \leq n \leq 2$ ) of protons might be coupled at different pH values. The Pourbaix diagram of  $\text{AQDS}(\text{NH}_4)_2$  (Figure 3b) was generated

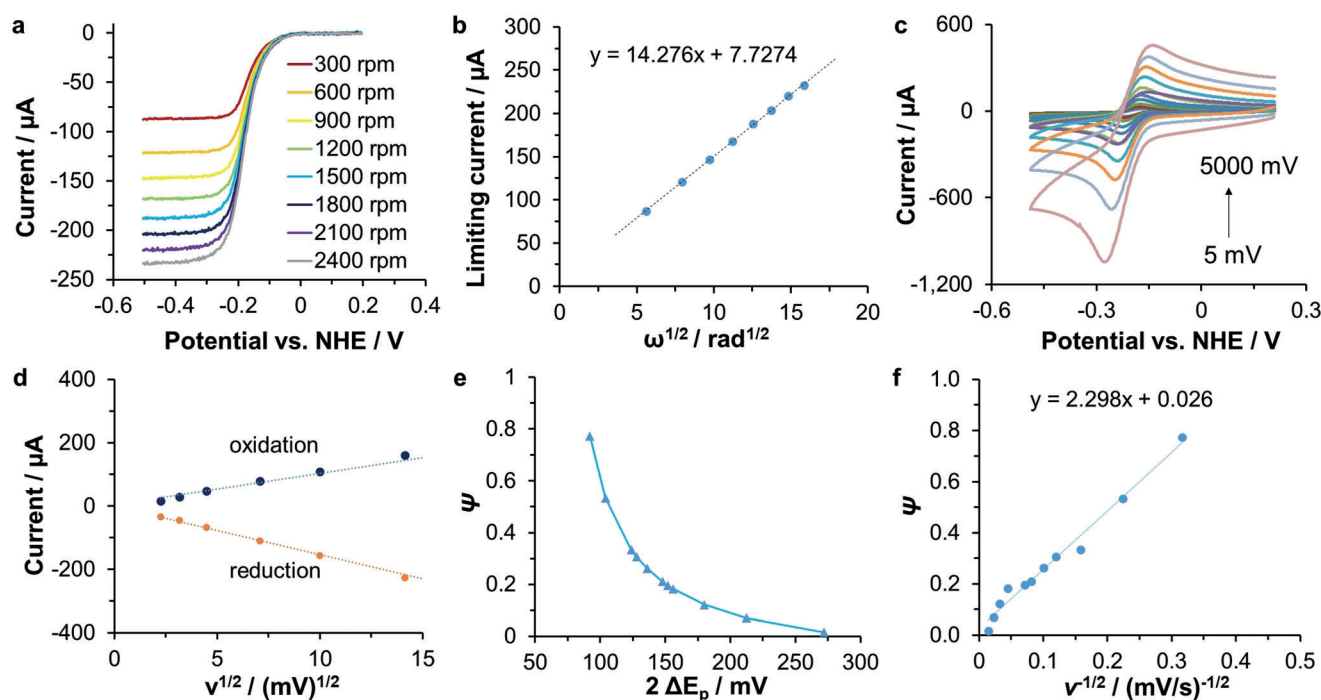
by measuring its redox potential at different pH value. To our surprise, the redox potential of  $\text{AQDS}(\text{NH}_4)_2$  kept nearly unchanged from pH 4 to 7, revealing the two-electron processes without being coupled by protons in this pH region. This phenomenon is attributed to the H-bonding interactions between ammonium cations and the carbonyl oxygen atoms of the AQDS anion. From pH 7 to 10, the redox potential linearly shifted to being more negative with a slope of  $-30 \text{ mV/pH}$  (Figure 3b). By using the Nernst equation, we can establish a relationship between the redox potential and the number of protons and electrons involved in the electrochemical reactions. Equation (2) showed the derivation of the Nernst equation for the reaction displayed in Equation (1), where  $z = 2$  in this case (two-electron process).



$$E = E^0 - \frac{RT}{zF} \ln \frac{1}{[\text{H}^+]^n} = E^0 - \frac{0.059n}{z} \text{pH} \quad (2)$$

According to Equation (2) where  $n$  was calculated as  $30 \text{ mV} * 2 / 0.059 \text{ V} = 1.02$ , the redox chemistry of  $\text{AQDS}(\text{NH}_4)_2$  in the region of pH 7–10 was assigned as a single proton-coupled 2 electron process. Meanwhile, peak to peak separation decreased with the increase of pH value as shown in Figure 3a, indicating gradually improved redox kinetics.

Electrochemical kinetics studies of  $\text{AQDS}(\text{NH}_4)_2$  were conducted by rotating disk electrode measurements and Nicholson analysis, as shown in Figure 4 (See experimental details



**Figure 4.** RDE test: (a) Linear sweep voltammograms of  $\text{AQDS}(\text{NH}_4)_2$  on a glassy carbon rotating disk electrode; (b) Levich plot of the limiting current vs. the square root of rotation rates for  $\text{AQDS}(\text{NH}_4)_2$ ; Conditions: 1.0 mM analyte in 0.5 M  $\text{NH}_4\text{l}$  electrolyte; scan rate:  $5 \text{ mVs}^{-1}$ ; rotation rates from 300 to 2400 rpm; working electrode, glassy carbon rotating disk electrode; counter electrode, glassy carbon; reference electrode, Ag/AgCl. Scan rate study and Nicholson's analysis of  $\text{AQDS}(\text{NH}_4)_2$ : (c) CV of  $\text{AQDS}(\text{NH}_4)_2$  at various scan rates (5, 10, 20, 50, 100, 200, 300, 500, 1000, 2000, 5000  $\text{mVs}^{-1}$ ). (d) The plot of  $i_c$  and  $i_a$  over the square root of scan rates for  $\text{AQDS}(\text{NH}_4)_2$  (blue trace for oxidative reaction, orange trace for reductive reaction); (e) Plot of  $\Psi$  versus  $2\Delta E_p$  of  $\text{AQDS}(\text{NH}_4)_2$ . (f) The linear relationship between  $\Psi$  and  $v^{1/2}$  of  $\text{AQDS}(\text{NH}_4)_2$ .



in supporting information). The diffusion coefficient was determined by the Levich equation [Eq. (3)]:

$$i_L = 0.620nFAC_0D^{2/3}\omega^{1/2}\nu^{-1/6} \quad (3)$$

where  $i_L$  is the limiting current from the RDE testing. The slope of  $i-\omega^{1/2}$  linear curve is  $0.620nFAC_0D^{2/3}\nu^{-1/6}$ .  $A$  is the area of the rotating electrode,  $n$  is the number of electrons involving the redox process,  $C_0$  is the concentration of compounds,  $D$  is the diffusion coefficient ( $\text{cm}^2\text{s}^{-1}$ ),  $\omega$  is the angular rotation rate of the electrode, and  $\nu$  is the kinematic viscosity. The calculated  $D$  value can be applied for electron transfer rate constant ( $k_0$ ) calculation using the Nicolson equation, Equation (4), in which  $\nu$  is the scan rate.

$$\Psi = k_0 \left( \frac{\pi D n F}{RT} \right)^{-1/2} \nu^{-1/2} \quad (4)$$

The  $\Psi$  value can be calculated by the well-known fitting Equation (5)

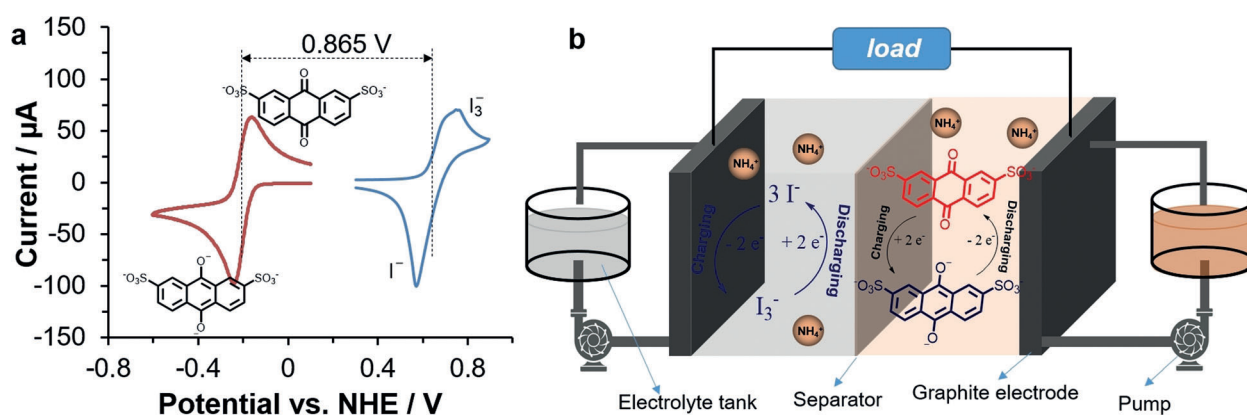
$$\Psi = \frac{-0.6288 + 0.0021n\Delta E_p}{1 - 0.017n\Delta E_p} \quad (5)$$

Where  $k_0$  is the electron transfer rate constant,  $\Delta E_p$  is the peak potential separation calculated by  $(E_{\text{oxidation}} - E_{\text{reduction}})$  at different scan rates (Figure 4d), and  $n$  equals 2 for a two electron process. The established linear relationship between  $\Psi$  and  $\nu^{-1/2}$  gives a slope of  $k_0(\pi D n F / RT)^{-1/2}$ , which can be used to calculate  $k_0$ . The Levich study and Nicolson measurements revealed the fast electrochemical kinetics of **AQDS-(NH<sub>4</sub>)<sub>2</sub>** at pH 7 with a diffusion coefficient and an electron transfer rate constant of  $4.55 \times 10^{-6} \text{ cm}^2\text{s}^{-1}$  and  $0.077 \text{ cm}^2\text{s}^{-1}$ , respectively. Besides, scan rate dependent studies of **AQDS-(NH<sub>4</sub>)<sub>2</sub>** (Figure 4d) also demonstrated that its reversible reduction/oxidation reactions are both diffusion controlled processes.

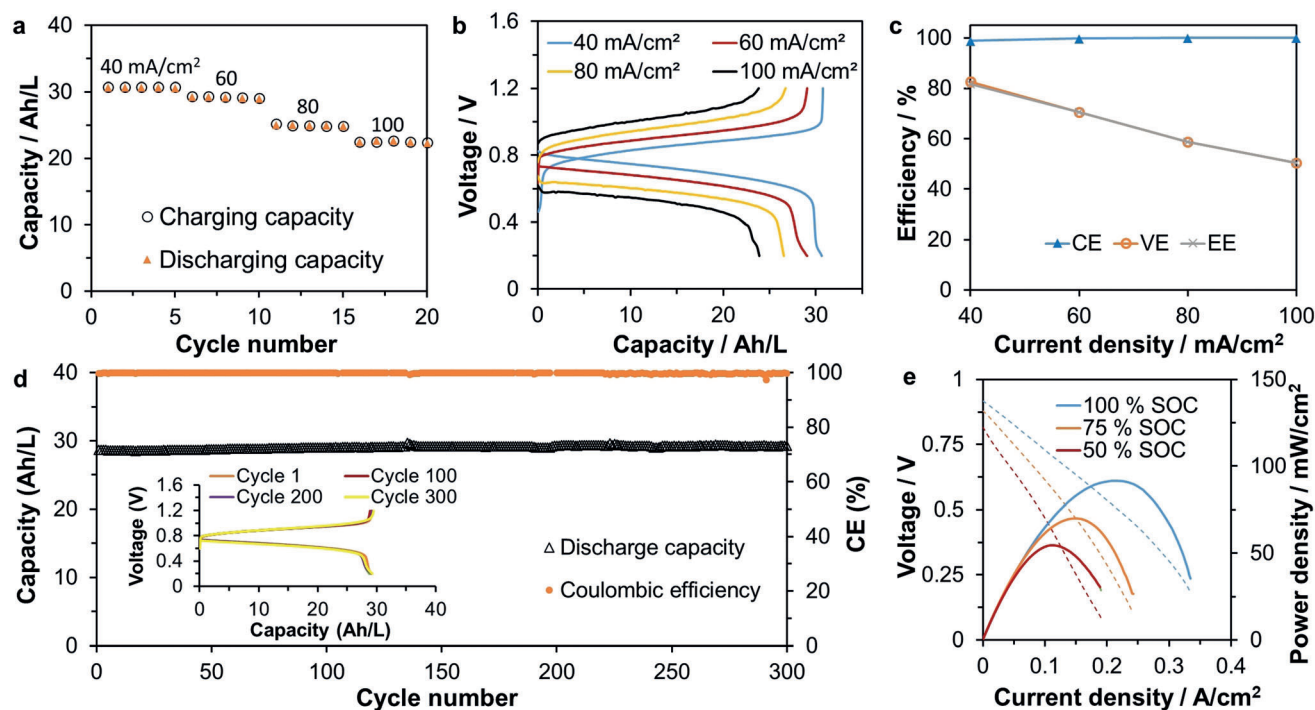
For the full AORFB demonstration, **NH<sub>4</sub>I** was selected as the cathode material due to its ammonium cation, excellent stability, and high solubility (ca. 10M in water). The resulted **AQDS-(NH<sub>4</sub>)<sub>2</sub>/NH<sub>4</sub>I** combination predicts a theoretical cell voltage of 0.865 V (Figure 5a). Considering the high solubility

of **AQDS-(NH<sub>4</sub>)<sub>2</sub>** and the two electron redox process, the **AQDS-(NH<sub>4</sub>)<sub>2</sub>/NH<sub>4</sub>I** AORFB could deliver a theoretical energy density as high as  $44 \text{ WhL}^{-1}$  for the full battery ( $30 \text{ WhL}^{-1}$  when 1M **NH<sub>4</sub>I** supporting electrolyte is used). However, we found that the solubility of the reduced state of **AQDS-(NH<sub>4</sub>)<sub>2</sub>** is around 0.8M in 0.5M **NH<sub>4</sub>I** supporting electrolyte at pH 7 as a more concentrated **AQDS-(NH<sub>4</sub>)<sub>2</sub>** anolyte would result in precipitation during the charging process. Thus, we systematically evaluated the cycling performance of an **AQDS-(NH<sub>4</sub>)<sub>2</sub>/NH<sub>4</sub>I** AORFB at 0.75M ( $1.5 \text{ M e}^-$ , a charge capacity of  $40.2 \text{ AhL}^{-1}$  and an energy density of  $12.5 \text{ WhL}^{-1}$ ). The cell design is outlined in Figure 5b, where a piece of Nafion 115 membrane was employed as the separator to allow the exchange of ammonium cation and avoid the crossover of anionic redox active species including **AQDS<sup>2-</sup>**, **I<sup>-</sup>**, and **I<sub>3</sub><sup>-</sup>**. 0.5M **NH<sub>4</sub>I** was added into anode as supporting electrolyte to improve the electrolyte conductivity. Up to 5 equivalent **NH<sub>4</sub>I** (compared to **AQDS-(NH<sub>4</sub>)<sub>2</sub>**) was used in cathode side to ensure the reliable evaluation of the limiting **AQDS-(NH<sub>4</sub>)<sub>2</sub>** anolyte side while enabling the fully **I<sub>2</sub>** complexing to generate soluble **I<sub>3</sub><sup>-</sup>**. Electrochemical impedance spectroscopy (EIS) revealed a high-frequency area specific resistance ( $R_{\text{int}}$ ) of the battery as low as  $1.44 \Omega \text{ cm}^2$  (Figure S11).

The current rate performance was investigated from  $40 \text{ mA cm}^{-2}$  to  $100 \text{ mA cm}^{-2}$  with an increment of  $20 \text{ mA cm}^{-2}$ . For each current density, 5 charge and discharge cycles were tested with cutoff voltages at 1.2 V for the charging process and 0.2 V for the discharging process. In our **AQDS-(NH<sub>4</sub>)<sub>2</sub>/NH<sub>4</sub>I** AORFB cycling experiments, we noticed the low coulombic efficiency (CE) and capacity retention during first several cycles (Figure S6) which is owing to the intermolecular dimerization between **AQDS-(NH<sub>4</sub>)<sub>2</sub>** and its reduced species (**AQDS-(NH<sub>4</sub>)<sub>4</sub>**).<sup>[18]</sup> It was reported that **AQDSH<sub>2</sub>** and its reduced species could form a dimer compound which cannot be utilized in the discharging process, thus hindering the full utilization of the active materials.<sup>[18]</sup> To support the hypothesis, in a mixed electrolyte of **AQDS-(NH<sub>4</sub>)<sub>2</sub>** and **AQDS-(NH<sub>4</sub>)<sub>4</sub>**, there was an additional oxidation observed at 0.2 V, assigned to the oxidation of the **AQDS-(NH<sub>4</sub>)<sub>2</sub>/AQDS-(NH<sub>4</sub>)<sub>4</sub>** dimer (Figure S7), whose exact structure remains to be elucidated. In the future, it is possible to avoid the dimerization using additives or structural modifi-



**Figure 5.** (a) Cyclic voltammogram of 4 mM **AQDS-(NH<sub>4</sub>)<sub>2</sub>** (in 0.5 M **NH<sub>4</sub>I**) and 4 mM **NH<sub>4</sub>I** (in 0.5 M **NH<sub>4</sub>Cl**), respectively (pH 7). (b) Schematic representation of the **AQDS-(NH<sub>4</sub>)<sub>2</sub>/NH<sub>4</sub>I** neutral AORFB and cell reactions.



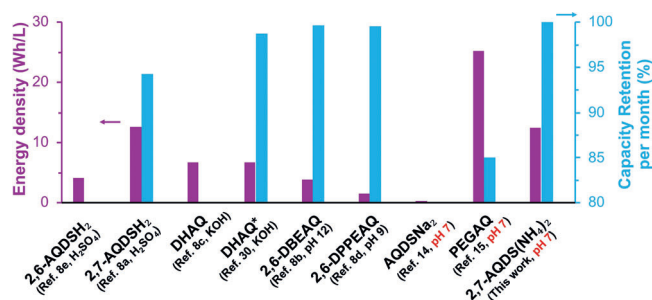
**Figure 6.** Battery performance of the 0.75 M  $\text{AQDS}(\text{NH}_4)_2/\text{NH}_4\text{I}$  neutral AORFB. (a) Capacity vs. the cycle number from 40 to 100  $\text{mA cm}^{-2}$  of the battery. 5 cycles' test was conducted for each current density. (b) Voltage versus capacity profile at different charging/discharging current density. (c) Averaged coulombic efficiency, voltage efficiency, and energy efficiency at different charging/discharging current density. (d) Capacity versus cycle number for 300 cycles. The battery is cycled at 60  $\text{mA cm}^{-2}$ . Inset: selected representative voltage versus capacity profiles. (e) Power density of the battery at various state of charge.

cations. As a result, the battery was firstly cycled at a current density of 40  $\text{mA cm}^{-2}$  until the CE reached 99% to avoid the inaccuracy of the rate performance evaluation due to the dimmer formation. Thereafter, the current rate dependent cycling was conducted. Overall,  $\text{AQDS}(\text{NH}_4)_2/\text{NH}_4\text{I}$  AORFB exhibited an excellent rate performance. As shown in Figure 6a, 5 stable cycles were demonstrated at each current density without capacity decay. At 40  $\text{mA cm}^{-2}$ , the battery presented a capacity utilization of 76.4% ( $30.7 \text{ Ah L}^{-1}$  out of  $40.2 \text{ Ah L}^{-1}$ ), which decreased to 72.3% when the current density was increased to 60  $\text{mA cm}^{-2}$  (Figure 6b) due to increased charging/discharging overpotential. Benefitted from low cell resistance, the battery exhibits an impressive energy efficiency up to 81.7% at 40  $\text{mA cm}^{-2}$  and 70.6% at 60  $\text{mA cm}^{-2}$  (Figure 6c), standing for the most energy efficient neutral AORFBs to date. In addition, a high power density of  $91.5 \text{ mW cm}^{-2}$  was recorded at 100% SOC (Figure 6e), which could be further optimized by applying more conductive ion exchange membranes and supporting electrolytes.

Long-term cycling was examined at 60  $\text{mA cm}^{-2}$  to further validate the cycling stability of the  $\text{AQDS}(\text{NH}_4)_2/\text{NH}_4\text{I}$  AORFB (Figure 6d), which was first cycled at 40  $\text{mA cm}^{-2}$  for a few cycles to stabilize the dimerization process. The battery delivered rather stable capacity retention as no capacity decay was detected after 300 cycles (ca. 15 days) and represent the most stable AQ based AORFBs. Judging from the well-overlapped charging/discharging profile (Figure 6d and Figure S8), the charging/discharging overpotential stayed the

same from the 10<sup>th</sup> to 300<sup>th</sup> cycle, which suggests no ohmic loss and good chemical compatibility with the membrane and other cell components. This is also in line with the almost identical  $R_{\text{int}}$  from the EIS measurements before and after cycling (Figure S12). The energy efficiency maintained about 70% during cycling (Figure S9). Post-cell analysis for the 0.75 M  $\text{AQDS}(\text{NH}_4)_2/\text{NH}_4\text{I}$  AORFB after 300 cycles were conducted using cyclic voltammetry,  $^1\text{H NMR}$  (Figure S10–S11). Both CV and  $^1\text{H NMR}$  studies indicated there was no chemical degradation for  $\text{AQDS}(\text{NH}_4)_2$ . In a stark contrast, even at the 0.1 M concentration, an  $\text{AQDSNa}_2/\text{NaI}$  AORFB could not be cycled because of the rapid precipitate formation of the charge state,  $\text{AQDSNa}_4$ , further highlighting the unique role of the  $\text{NH}_4^+$  cations for  $\text{AQDS}(\text{NH}_4)_2$ .

As shown in Figure 7, representative AQ based AORFBs are compared in the aspects of demonstrated energy density and normalized stability (per month). It is clear that the demonstrated pH neutral  $\text{AQDS}(\text{NH}_4)_2/\text{NH}_4\text{I}$  AORFB displayed much improved performance compared to reported AQDS based AORFBs in terms of energy density and cycling stability. The acid or alkaline AQ based AORFBs suffer either low energy density or poor cycling stability, which attribute to the low solubility or poor chemical stability of active materials. As a result of the extraordinary chemical stability and solubility of  $\text{AQDS}(\text{NH}_4)_2$  in the neutral supporting electrolyte, the pH neutral AORFB  $\text{AQDS}(\text{NH}_4)_2/\text{NH}_4\text{I}$  system demonstrated an energy density of  $12.5 \text{ Wh/L}$  and the capacity retention of ca. 100% per month, representing one of the most energy dense and stable AORFBs reported to



**Figure 7.** Comparison of demonstrated energy densities and capacity retention per month of the selected AQ based AORFBs (\* stands for the RFB with redox state management. Capacity retention lower than 80% per month was not displayed in the Figure).

date. Recently, a water-miscible anthraquinone (PEGAQ) molecule with 2-(2-(2-hydroxyethoxy)ethoxy)ethoxy side chains was reported, which stands for one of the most water soluble anthraquinone derivatives.<sup>[15]</sup> The neutral PEGAQ/Fe(CN)<sup>2-</sup> AORFB was demonstrated with an energy density as high as 25.2 WhL<sup>-1</sup>. However, the cycling capacity retention of the battery was only 85% per month due to the decomposition of PEGAQ.

## Conclusion

In summary, we have developed a new ammonium functionalized anthraquinone derivative (AQDS(NH<sub>4</sub>)<sub>2</sub>) as the anolyte material for pH neutral AORFB application. The synthesis of AQDS(NH<sub>4</sub>)<sub>2</sub> is straightforward and convenient at ambient conditions, and scalable using common commercial precursors. In addition to its hydrophilic nature, the introduced ammonium cations form hydrogen bonds with the AQDS<sup>2-</sup> anion to improve its solubility. Paired with the highly soluble NH<sub>4</sub>I cathode material, the demonstrated AQDS-(NH<sub>4</sub>)<sub>2</sub>/NH<sub>4</sub>I battery stands for the most stable pH neutral, metal free anthraquinone AORFB with very high capacity and energy density. Taking account of the easy synthesis, low cost, high energy density, excellent stability and environmental advantage, AQDS(NH<sub>4</sub>)<sub>2</sub> can be regarded as a highly attractive anolyte molecule in AORFBs for large scale sustainable energy storage. Moreover, the present chemistry of AQDS(NH<sub>4</sub>)<sub>2</sub> opens a new avenue to utilizing anthraquinone compounds in developing pH neutral, benign and stable cycling AORFBs to promise low cost and sustainable green energy storage.

## Experimental Section

**Synthesis of AQDS(NH<sub>4</sub>)<sub>2</sub>:** 9,10-Anthraquinone-2,6-disulfonic acid disodium salt (20.0 g, 48.5 mmol) was dissolved in 100 mL deionized water and flushed over a cation exchange column with Amberlite cation exchange resin (IR-120 hydrogen form). The obtained 9,10-Anthraquinone-2,6-disulfonic acid solution was cooled down by an ice bath. Then 10 mL 30% ammonium hydroxide was added to convert the acid to ammonium salt. After the water was removed by a rotary evaporator, the wet solid residue was dried in a vacuum oven at 70°C overnight. The final product was collected as dark brown

solid (19.1 g, 98.5%). <sup>1</sup>H-NMR (500 MHz, D<sub>2</sub>O): δ = 8.29 (d, 2H), 8.02 (dd, 2H), 7.94 ppm (d, 2H). Anal. Calcd for C<sub>14</sub>H<sub>14</sub>O<sub>8</sub>N<sub>2</sub>S<sub>2</sub>: C, 41.76; H, 3.48; N, 6.96. Found C, 42.03; H, 3.51; N, 6.28.

**Synthesis of AQDSNH<sub>4</sub>:** 9,10-Anthraquinone-2-disulfonic acid sodium salt (3.0 g, 9.7 mmol) and 30 mL Amberlite cation exchange resin (IR-120 hydrogen form) were added in 50 mL deionized water. The mixture was stirred overnight when all anthraquinone was dissolved. Then the mixture was filtered, and the filtrate was flushed over a cation exchange column with Amberlite cation exchange resin (IR-120 hydrogen form) again. Following steps are the same as the synthesis of AQDS(NH<sub>4</sub>)<sub>2</sub>. The product was obtained as light yellow powder with a yield of 98%. <sup>1</sup>H-NMR (500 MHz, D<sub>2</sub>O): δ = 8.29 (d, 2H), 8.02 (dd, 2H), 7.94 ppm (d, 2H). Anal. Calcd for C<sub>14</sub>H<sub>11</sub>O<sub>5</sub>NS: C, 55.08; H, 3.63; N, 4.59. Found C, 55.31; H, 3.94; N, 4.57.

**Flow cell tests:** Flow cells for the RFBs were constructed with two carbon electrolyte chambers, two graphite felt electrodes (SGL Carbon Group, Germany), a piece of Nafion 115 membrane sandwiched between graphite felts, and two copper current collectors. The Nafion membranes were boiled in 1 M H<sub>2</sub>SO<sub>4</sub> solution for 2 hours, 30% H<sub>2</sub>O<sub>2</sub> solution for 2 hours, and then immersed in 0.5 M NH<sub>4</sub>I aqueous solution overnight. The membranes are rinsed with DI water before use. All other components were dried at 80°C for 2 hours. 18 mL 2.25 M NH<sub>4</sub>I aqueous solution was employed as catholyte. 12 mL 0.75 M AQDS(NH<sub>4</sub>)<sub>2</sub> in 0.75 M NH<sub>4</sub>I solution was used as anolyte. The pH values of both catholyte and anolyte were adjusted to be 7 by ammonium hydroxide. When assembling the battery, each carbon chamber was connected with an electrolyte reservoir using a piece of Viton tubing. The electrolyte reservoir is home designed and is a 10 mL glass tube (2 cm inner diameter). The active area of the cell was 10 cm<sup>2</sup>. A Masterflex L/S peristaltic pump (Cole-Parmer, Vernon Hills, IL) was used to press the Viton tubing to circulate the electrolytes through the electrodes at a flow rate of 60 mL min<sup>-1</sup>. Both reservoirs were purged with nitrogen to remove O<sub>2</sub> and then sealed before cell cycling. The flow cell was galvanostatically charged/discharged at room temperature on a battery tester (Land Instruments) in an argon filled glovebox with an oxygen content lower than 1 ppm. The voltage range was set between 1.2 V to 0.2 V and the current densities ranged from 40 to 100 mA cm<sup>-2</sup>.

## Acknowledgements

We thank the National Science Foundation Career Award (Grant No. 1847674), faculty startup funds from Utah State University, and the Utah Science Technology and Research initiative (USTAR) UTAG award for providing financial support for our flow battery project. B.H. is grateful to the China CSC Fellowship supported by the China CSC Study Abroad program and Utah Energy Triangle Student Award for supporting his graduate program. M.H. is grateful to the China CSC Fellowship supported by the China CSC Study Abroad program for supporting her graduate program. B.Y. acknowledges the China CSC Study Abroad program for supporting her exchange study at USU.

## Conflict of interest

The authors declare no conflict of interest.

**Stichwörter:** Ammoniumionen · Anthrachinon · Energiespeicherung · Redox-Flow-Batterien

- [1] <https://www.esrl.noaa.gov/gmd/ccgg/trends/index.html>, **2018**.
- [2] B. Dunn, H. Kamath, J.-M. Tarascon, *Science* **2011**, *334*, 928–935.
- [3] a) G. L. Soloveichik, *Chem. Rev.* **2015**, *115*, 11533–11558; b) W. Wang, Q. T. Luo, B. Li, X. L. Wei, L. Y. Li, Z. G. Yang, *Adv. Funct. Mater.* **2013**, *23*, 970–986; c) „Redox-Active Inorganic Materials for Redox Flow Batteries“: B. Hu, J. Luo, C. Debruler, M. Hu, W. Wu, T. L. Liu, in *Ency. Inorg. Bioinorg. Chem: Inorganic Battery Materials*, **2019**.
- [4] a) J. Winsberg, T. Hagemann, T. Janoschka, M. D. Hager, U. S. Schubert, *Angew. Chem. Int. Ed.* **2017**, *56*, 686–711; *Angew. Chem.* **2017**, *129*, 702–729; b) J. Luo, B. Hu, M. Hu, Y. Zhao, T. L. Liu, *ACS Energy Lett.* **2019**, <https://doi.org/10.1021/acscenergylett.9b01332>; c) X. Wei, W. Pan, W. Duan, A. Hollas, Z. Yang, B. Li, Z. Nie, J. Liu, D. Reed, W. Wang, V. Sprenkle, *ACS Energy Lett.* **2017**, *2*, 2187–2204; d) Y. Ding, C. Zhang, L. Zhang, Y. Zhou, G. Yu, *Chem. Soc. Rev.* **2018**, *47*, 69–103.
- [5] a) T. Janoschka, N. Martin, U. Martin, C. Friebe, S. Morgenstern, H. Hiller, M. D. Hager, U. S. Schubert, *Nature* **2015**, *527*, 78–81; b) T. B. Liu, X. L. Wei, Z. M. Nie, V. Sprenkle, W. Wang, *Adv. Energy Mater.* **2016**, *6*, 1501449; c) T. Janoschka, N. Martin, M. D. Hager, U. S. Schubert, *Angew. Chem. Int. Ed.* **2016**, *55*, 14427–14430; *Angew. Chem.* **2016**, *128*, 14639–14643; d) B. Hu, C. DeBruler, Z. Rhodes, T. L. Liu, *J. Am. Chem. Soc.* **2017**, *139*, 1207–1214; e) C. DeBruler, B. Hu, J. Moss, X. Liu, J. Luo, Y. Sun, T. L. Liu, *Chem* **2017**, *3*, 961–978; f) B. Hu, Y. Tang, J. Luo, G. Grove, Y. Guo, T. L. Liu, *Chem. Commun.* **2018**, *54*, 6871–6874; g) J. Luo, B. Hu, C. Debruler, T. L. Liu, *Angew. Chem. Int. Ed.* **2018**, *57*, 231–235; *Angew. Chem.* **2018**, *130*, 237–241; h) J. Luo, B. Hu, C. Debruler, Y. Bi, Y. Zhao, B. Yuan, M. Hu, W. Wu, T. L. Liu, *Joule* **2019**, *4*, 1; i) J. Luo, W. Wu, C. Debruler, B. Hu, M. Hu, T. L. Liu, *J. Mater. Chem. A* **2019**, *7*, 9130–9136; j) W. Liu, Y. Liu, H. Zhang, C. Xie, L. Shi, Y.-G. Zhou, X. Li, *Chem. Commun.* **2019**, *55*, 4801–4804.
- [6] a) L. Cosimbescu, X. L. Wei, M. Vijayakumar, W. Xu, M. L. Helm, S. D. Burton, C. M. Sorensen, J. Liu, V. Sprenkle, W. Wang, *Sci. Rep.* **2015**, *5*, 14117; b) E. S. Beh, D. De Porcellinis, R. L. Gracia, K. T. Xia, R. G. Gordon, M. J. Aziz, *ACS Energy Lett.* **2017**, *2*, 639–644; c) Y. Ding, Y. Zhao, Y. Li, J. B. Goodenough, G. Yu, *Energy Environ. Sci.* **2017**, *10*, 491–497; d) G. Cong, Y. Zhou, Z. Li, Y.-C. Lu, *ACS Energy Lett.* **2017**, *2*, 869–875; e) Y. Zhao, Y. Ding, J. Song, G. Li, G. Dong, J. B. Goodenough, G. Yu, *Angew. Chem. Int. Ed.* **2014**, *53*, 11036–11040; *Angew. Chem.* **2014**, *126*, 11216–11220; f) F. Pan, J. Yang, Q. Huang, X. Wang, H. Huang, Q. Wang, *Adv. Energy Mater.* **2014**, *4*, 1400567; g) M. Zhou, Q. Huang, T. N. Pham Truong, J. Ghilane, Y. G. Zhu, C. Jia, R. Yan, L. Fan, H. Randriamahazaka, Q. Wang, *Chem* **2017**, *3*, 1036–1049.
- [7] C. S. Sevov, D. P. Hickey, M. E. Cook, S. G. Robinson, S. Barnett, S. D. Minter, M. S. Sigman, M. S. Sanford, *J. Am. Chem. Soc.* **2017**, *139*, 2924.
- [8] a) B. Huskinson, M. P. Marshak, C. Suh, S. Er, M. R. Gerhardt, C. J. Galvin, X. D. Chen, A. Aspuru-Guzik, R. G. Gordon, M. J. Aziz, *Nature* **2014**, *505*, 195–199; b) D. G. Kwabi, K. Lin, Y. Ji, E. F. Kerr, M.-A. Goulet, D. De Porcellinis, D. P. Tabor, D. A. Pollack, A. Aspuru-Guzik, R. G. Gordon, M. J. Aziz, *Joule* **2018**, *2*, 1894–1906; c) K. X. Lin, Q. Chen, M. R. Gerhardt, L. C. Tong, S. B. Kim, L. Eisenach, A. W. Valle, D. Hardee, R. G. Gordon, M. J. Aziz, M. P. Marshak, *Science* **2015**, *349*, 1529–1532; d) Y. Ji, M.-A. Goulet, D. A. Pollack, D. G. Kwabi, S. Jin, D. De Porcellinis, E. F. Kerr, R. G. Gordon, M. J. Aziz, *Adv. Energy Mater.* **2019**, *9*, 1900039; e) B. Yang, L. Hooper-Burkhardt, F. Wang, G. K. S. Prakash, S. R. Narayanan, *J. Electrochem. Soc.* **2014**, *161*, A1371–A1380; f) L. Hooper-Burkhardt, S. Krishnamoorthy, B. Yang, A. Murali, A. Nirmalchandar, G. K. S. Prakash, S. R. Narayanan, *J. Electrochem. Soc.* **2017**, *164*, A600–A607; g) J. Huang, Z. Yang, M. Vijayakumar, W. Duan, A. Hollas, B. Pan, W. Wang, X. Wei, L. Zhang, *Adv. Sustainable Syst.* **2018**, *2*, 1700131.
- [9] X. Wei, W. Xu, M. Vijayakumar, L. Cosimbescu, T. Liu, V. Sprenkle, W. Wang, *Adv. Mater.* **2014**, *26*, 7649–7653.
- [10] a) K. Lin, R. Gómez-Bombarelli, E. S. Beh, L. Tong, Q. Chen, A. Valle, A. Aspuru-Guzik, M. J. Aziz, R. G. Gordon, *Nat. Energy* **2016**, *1*, 16102; b) A. Orita, M. G. Verde, M. Sakai, Y. S. Meng, *Nat. Commun.* **2016**, *7*, 13230; c) A. Hollas, X. Wei, V. Murugesan, Z. Nie, B. Li, D. Reed, J. Liu, V. Sprenkle, W. Wang, *Nat. Energy* **2018**, *3*, 508–514; d) J. D. Milshtein, A. P. Kaur, M. D. Casselman, J. A. Kowalski, S. Modekrutti, P. Zhang, N. H. Attanayake, C. F. Elliott, S. R. Parkin, C. Risko, F. R. Brushett, S. A. Odom, *Energy Environ. Sci.* **2016**, *9*, 3531–3543; e) N. H. Attanayake, J. A. Kowalski, K. V. Greco, M. D. Casselman, J. D. Milshtein, S. J. Chapman, S. R. Parkin, F. R. Brushett, S. A. Odom, *Chem. Mater.* **2019**, *31*, 4353–4363.
- [11] a) C. Yang, G. Nikiforidis, J. Y. Park, J. Choi, Y. Luo, L. Zhang, S.-C. Wang, Y.-T. Chan, J. Lim, Z. Hou, M.-H. Baik, Y. Lee, H. R. Byon, *Adv. Energy Mater.* **2018**, *8*, 170289; b) J. Huang, L. Cheng, R. S. Assary, P. Wang, Z. Xue, A. K. Burrell, L. A. Curtiss, L. Zhang, *Adv. Energy Mater.* **2015**, *5*, 1401782; c) S. E. Doris, A. L. Ward, A. Baskin, P. D. Frischmann, N. Gavvalapalli, E. Chénard, C. S. Sevov, D. Prendergast, J. S. Moore, B. A. Helms, *Angew. Chem. Int. Ed.* **2017**, *56*, 1595–1599; *Angew. Chem.* **2017**, *129*, 1617–1621.
- [12] a) M. R. Gerhardt, L. Tong, R. Gómez-Bombarelli, Q. Chen, M. P. Marshak, C. J. Galvin, A. Aspuru-Guzik, R. G. Gordon, M. J. Aziz, *Adv. Energy Mater.* **2017**, *7*, 1601488; b) M.-A. Goulet, M. J. Aziz, *J. Electrochem. Soc.* **2018**, *165*, A1466–A1477; c) M.-A. Goulet, L. Tong, D. A. Pollack, D. P. Tabor, S. A. Odom, A. Aspuru-Guzik, E. E. Kwan, R. G. Gordon, M. J. Aziz, *J. Am. Chem. Soc.* **2019**, *141*, 8014–8019.
- [13] J. Luo, A. Sam, B. Hu, C. DeBruler, X. Wei, W. Wang, T. L. Liu, *Nano Energy* **2017**, *42*, 215–221.
- [14] W. Lee, A. Permatasari, B. W. Kwon, Y. Kwon, *Chem. Eng. J.* **2019**, *358*, 1438–1445.
- [15] S. Jin, Y. Jing, D. G. Kwabi, Y. Ji, L. Tong, D. De Porcellinis, M.-A. Goulet, D. A. Pollack, R. G. Gordon, M. J. Aziz, *ACS Energy Lett.* **2019**, *4*, 1342–1348.
- [16] J. Carretero-González, E. Castillo-Martínez, M. Armand, *Energy Environ. Sci.* **2016**, *9*, 3521–3530.
- [17] J. A. N. F. Gomes, R. B. Mallion, *Chem. Rev.* **2001**, *101*, 1349–1384.
- [18] T. J. Carney, S. J. Collins, J. S. Moore, F. R. Brushett, *Chem. Mater.* **2017**, *29*, 4801–4810.

Manuskript erhalten: 25. Juni 2019  
Akzeptierte Fassung online: 5. August 2019  
Endgültige Fassung online: ■ ■ ■ ■ ■ ■ ■ ■ ■ ■


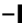



## Forschungsartikel

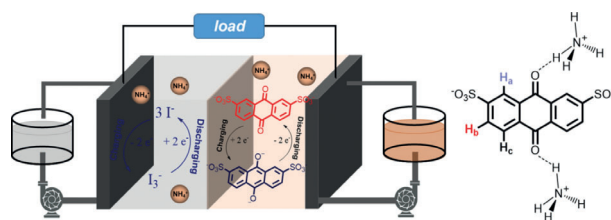


## Redox-Flow-Batterien

B. Hu, J. Luo, M. Hu, B. Yuan,

T. L. Liu\*     

A pH-Neutral, Metal-Free Aqueous Organic Redox Flow Battery Employing an Ammonium Anthraquinone Anolyte



Ein Anthrachinonsalz, AQDS(NH<sub>4</sub>)<sub>2</sub>, wurde als neues Anolytmaterial für pH-neutrale wässrige organische Redox-Flow-Batterien (AORFBs) mit einer Löslichkeit von 1.9 M in Wasser konzipiert. Eine mit AQDS(NH<sub>4</sub>)<sub>2</sub> gefertigte AORFB

zeigte eine hervorragende Akkuleistung, einschließlich 100% Zyklenfestigkeit über 300 Zyklen, eine Energieeffizienz von 70.6% bei 60 mA cm<sup>-2</sup> und eine Leistungsdichte von 91.5 mW cm<sup>-2</sup> bei 100% Ladezustand.

